INTERNATIONAL JOURNAL FOR NUMERICAL METHODS IN FLUIDS, VOL. 8, 97–119 (1988)

FLUX DIFFERENCE SPLITTING FOR THE EULER EQUATIONS IN ONE SPATIAL CO-ORDINATE WITH AREA VARIATION

P. GLAISTER

Department of Mathematics, P.O. Box 220, University of Reading, Whiteknights, Reading, Berkshire, RG6 2AX, U.K.

SUMMARY

An approximate (linearized) Riemann solver is presented for the solution of the Euler equations of gas dynamics in one spatial co-ordinate. This includes cylindrically and spherically symmetric geometries and also applies to narrow ducts with area variation. The method is Roe's flux difference splitting with a technique for dealing with source terms. The results of two problems, a spherically divergent infinite shock and a converging cylindrical shock, are presented. The numerical results compare favourably with those of Noh's recent survey and also with those of Ben-Artzi and Falcovitz using a more complicated Riemann solver.

KEY WORDS Approximate Riemann solver Euler equations Duct flows

1. INTRODUCTION

Recently, much success has been enjoyed by numerical schemes for hyperbolic conservation laws that update the solution by appealing to the information obtained by solving local Riemann problems at the interface between computational cells. It is possible in this way to obtain very accurate solutions for inviscid compressible flow in a straight pipe. In that case, the Riemann problems to be solved are 'classical'; they are governed by the homogeneous (source-free) Euler equations and the data is piecewise constant. To generalize the technique (in the first place to non-homogeneous flows), one possibility is to construct and solve 'generalized Riemann problems' governed by the non-homogeneous equations and possibly having non-constant data either side of the initial discontinuity. Such generalized Riemann problems are obtained with considerable analytical effort and add complexity and expense to the calculations. It is therefore of interest to know whether such generalized Riemann problems are an essential contribution towards the creation of more general codes or whether the required information is obtainable from solutions to the classical problem.

For homogeneous equations, the classical problem can provide all the information needed to obtain second-order accuracy (see References 1 and 2). In the present paper we derive a scheme which solves to second-order accuracy a class of non-homogeneous equations including the Euler equations with cylindrical or spherical symmetry or with source terms arising from variation of area along a narrow duct. However, the only Riemann problems solved are classical.

In §2 we review the equations for the flow of an inviscid perfect gas in a general orthogonal curvilinear co-ordinate system. This is done in order to make clear the origin of the non-Cartesian terms in the subsequent equations. In §3 we describe the details of the flux difference splitting scheme for the approximate solution of the equations given in §2, in the case of an ideal gas whose

0271–2091/88/010097–23$11.50

Received 17 December 1986
Revised 24 March 1987

flow can be described by one curvilinear space co-ordinate only. In §4 we discuss the properties of the scheme given in §3, while in §5 we describe two specific test problems that can be used to test such schemes. Finally in §6 we display the numerical results achieved for these two problems and compare them with solutions obtained by existing algorithms.

2. EQUATIONS OF FLOW

In this section we consider the Euler equations for modelling the time-dependent flow of an inviscid, compressible fluid that may be described by one of the co-ordinates in a general orthogonal curvilinear co-ordinate system (x_1, x_2, x_3).

2.1

We first state the system of differential equations describing the motion of an ideal gas in the form

$$\rho_t + \operatorname{div}(\rho \mathbf{u}) = 0, \tag{1}$$

$$(\rho \mathbf{u})_t + \operatorname{div}(\rho \mathbf{u}\mathbf{u}) = -\operatorname{grad} p, \tag{2}$$

$$e_t + \operatorname{div}[\mathbf{u}(e+p)] = 0 \tag{3}$$

together with

$$e = \frac{p}{\gamma - 1} + \tfrac{1}{2}\rho \mathbf{u}\cdot\mathbf{u}, \tag{4}$$

where $\rho = \rho(\mathbf{x}, t)$, $\mathbf{u} = \mathbf{u}(\mathbf{x}, t) = [u_1(\mathbf{x}, t), u_2(\mathbf{x}, t), u_3(\mathbf{x}, t)]^{\mathrm{T}}$ and $e = e(\mathbf{x}, t)$ represent the density, velocity in the three co-ordinate directions and the total energy, respectively, at a general position in space $\mathbf{x} = (x_1, x_2, x_3)^{\mathrm{T}}$ and at time t. The ratio of specific heat capacities of the fluid is represented by γ.

We notice the emergence of a 'non-divergence' term in equation 2—namely, grad p—which takes this particular form because the stress tensor is diagonal. Now for a general orthogonal curvilinear co-ordinate system |grad| and div are generally different (although they are identical for one-dimensional Cartesian geometry). Thus care has to be taken when we are working in a co-ordinate system other than Cartesian—e.g., spherical polars—since equations (1)–(3) do not appear in the standard conservation form for the application of conservative finite difference techniques.

2.2

If we now consider flow that is wholly dependent on one of the co-ordinate directions, say x_1, then equations (1)–(4) become

$$\rho_t + \frac{1}{h_1 h_2 h_3}\frac{\partial}{\partial x_1}(h_2 h_3 \rho u) = 0, \tag{5}$$

$$(\rho u)_t + \frac{1}{h_1 h_2 h_3}\frac{\partial}{\partial x_1}(h_2 h_3 \rho u^2) = -\frac{1}{h_1}\frac{\partial p}{\partial x_1}, \tag{6}$$

$$e_t + \frac{1}{h_1 h_2 h_3}\frac{\partial}{\partial x_1}[h_2 h_3 u(e+p)] = 0 \tag{7}$$

together with

$$e = \frac{p}{\gamma - 1} + \tfrac{1}{2}\rho u^2, \tag{8}$$

where h_1, h_2, h_3 are given as usual by the line element ds with

$$\mathrm{ds} = h_1\,\mathrm{d}x_1\,\hat{\mathbf{x}}_1 + h_2\,\mathrm{d}x_2\,\hat{\mathbf{x}}_2 + h_3\,\mathrm{d}x_3\,\hat{\mathbf{x}}_3.$$

Here $\hat{\mathbf{x}}_i$ is the unit vector parallel to the co-ordinate lines with x_i increasing, $\rho = \rho(x_1, t)$, $\mathbf{u} = [u(x_1, t), 0, 0]^{\mathrm{T}}$, $p = p(x_1, t)$ and $e = e(x_1, t)$. Equations (5)–(8) cannot now, however, be written directly in the standard conservation form

$$\mathbf{w}_t + [\mathbf{f}(\mathbf{w})]_{x_1} = \mathbf{0}, \tag{9}$$

with $\mathbf{w} = (\rho, \rho u, e)^{\mathrm{T}}$ and $\mathbf{f}$ a suitable vector-valued flux function. They can, however, be put in the form

$$(h_1 h_2 h_3 \rho)_t + (h_2 h_3 \rho u)_{x_1} = 0, \tag{10}$$

$$(h_1 h_2 h_3 \rho u)_t + (h_2 h_3 \rho u^2)_{x_1} = -h_2 h_3 \frac{\partial p}{\partial x_1}, \tag{11}$$

$$(h_1 h_2 h_3 e)_t + [h_2 h_3 u(e + p)]_{x_1} = 0. \tag{12}$$

In particular, in the case $h_1 = 1$, these equations can be written

$$(h_1 h_2 h_3 \rho)_t + (h_1 h_2 h_3 \rho u)_{x_1} = 0, \tag{13}$$

$$(h_1 h_2 h_3 \rho u)_t + [h_1 h_2 h_3 (p + \rho u^2)]_{x_1} = p \frac{\partial}{\partial x_1}(h_1 h_2 h_3), \tag{14}$$

$$(h_1 h_2 h_3 e)_t + [h_1 h_2 h_3 u(e + p)]_{x_1} = 0 \tag{15}$$

and it is these equations we now study together with

$$e = \frac{p}{\gamma - 1} + \tfrac{1}{2}\rho u^2. \tag{16}$$

Equations (13)–(16) are nearer to a 'conservation' like form but with an additional 'source'-like term on the right-hand side.

Now in a general orthogonal curvilinear co-ordinate system, $\mathrm{d}V = h_1 h_2 h_3\,\mathrm{d}x_1\,\mathrm{d}x_2\,\mathrm{d}x_3$ and thus equations (10)–(12) could also have been derived from the integral form of equations (1)–(3), where a quantity such as $h_1 h_2 h_3 \rho\,\mathrm{d}x_1\,\mathrm{d}x_2\,\mathrm{d}x_3$ represents the mass in a control volume bounded by surfaces $h_1 = \text{constant}$, $h_2 = \text{constant}$ and $h_3 = \text{constant}$.

2.3

An example of a flow described by the above equations when $h_1 = 1$ and the flow is wholly dependent on x_1 is that of an inviscid, compressible fluid through a duct of smoothly varying cross-section, often referred to as 'duct flow'. In that case we have

$$[S(r)\rho]_t + [S(r)\rho u]_r = 0, \tag{17}$$

$$[S(r)\rho u]_t + [S(r)(p + \rho u^2)]_r = pS'(r), \tag{18}$$

$$[S(r)e]_t + [S(r)u(e + p)]_r = 0 \tag{19}$$

together with

$$e = \frac{p}{\gamma - 1} + \tfrac{1}{2}\rho u^2, \tag{20}$$

where we write $x_1 = r$ for notational simplicity and $S(r)$ represents the cross-section of the duct at r, and $S(r) = h_1 h_2 h_3$.

More importantly, equations (17)–(20) cover all one-dimensional flows, including, for example, cylindrical and spherical flows with axial or radial symmetry. They also reduce to the correct form in the case $S \equiv 1$ (slab symmetry).

Equations (17)–(19) can be written as the system

$$S(r)\mathbf{w}_t + [S(r)\mathbf{f}(\mathbf{w})]_r = \mathbf{g}(\mathbf{w}), \tag{21}$$

where

$$\mathbf{w} = \begin{pmatrix} \rho \\ \rho u \\ e \end{pmatrix}, \quad \mathbf{f}(\mathbf{w}) = \begin{pmatrix} \rho u \\ p + \rho u^2 \\ u(e+p) \end{pmatrix} \quad \text{and} \quad \mathbf{g}(\mathbf{w}) = \begin{pmatrix} 0 \\ pS'(r) \\ 0 \end{pmatrix}. \tag{22}$$

We notice that $S(r)\mathbf{f}(\mathbf{w}) = \mathbf{f}[S(r)\mathbf{w}] = \mathbf{F}(\mathbf{W})$ and $S(r)\mathbf{w}_t = [S(r)\mathbf{w}]_t$, so that equations (21) and (22) can be rewritten immediately in the more familiar form

$$\mathbf{W}_t + [\mathbf{F}(\mathbf{W})]_r = \mathbf{g}(\mathbf{w}), \tag{23}$$

where $\mathbf{W} = S(r)\mathbf{w}$. This gives rise to new 'conserved' variables $\mathscr{R}$, M and E, where $\mathscr{R} = S(r)\rho$, $M = S(r)m$ and $E = S(r)e$. (Here m denotes the momentum ρu.) It also gives a new 'pressure' variable $P = S(r)p$. Quantities with the dimension of velocity are unaltered; e.g., the velocity $u = U$, sound speed $a = \sqrt{(\gamma p/\rho)} = \sqrt{(\gamma P/\mathscr{R})}$ and enthalpy $h = (e+p)/\rho = (E+P)/\mathscr{R} = H$. In particular, the matrix $\mathbf{A} = \partial\mathbf{F}(\mathbf{W})/\partial\mathbf{W}$ involves only velocities and is the same as $\partial\mathbf{f}(\mathbf{w})/\partial\mathbf{w}$.

Using these new variables, the Euler equations for duct flow become

$$\begin{pmatrix} \mathscr{R} \\ \mathscr{R}U \\ E \end{pmatrix}_t + \begin{pmatrix} \mathscr{R}U \\ P + \mathscr{R}U^2 \\ U(E+P) \end{pmatrix}_r = \begin{pmatrix} 0 \\ \dfrac{S'(r)}{S(r)}P \\ 0 \end{pmatrix}, \tag{24}$$

with

$$E = \frac{P}{\gamma - 1} + \tfrac{1}{2}\mathscr{R}U^2. \tag{25}$$

Equations (24) and (25) represent a system of hyperbolic 'conservation' laws similar to equations (21) for slab symmetry—i.e., when $S = 1$ and $\mathbf{g} = \mathbf{0}$— with an additional source term on the right-hand side. This additional term is due to the difference between the divergence and |gradient| operators in a non-Cartesian co-ordinate system in one dimension. The extra pressure term is due to the non-parallel nature of the sides of a control volume in the duct; i.e., on the non-cancelling of pressure terms on either side of the duct.

In the next section we describe a finite difference approximation for equations (24) and (25) using the linearized Riemann solver of Roe.[3]

3. FLUX DIFFERENCE SPLITTING

In this section we consider a finite difference approximation for the solution of equations (24) and (25).

3.1

In the case of slab symmetry, $S \equiv 1$, equations (24) and (25) reduce to the one-dimensional Euler equations in a single Cartesian co-ordinate, which can be solved by flux difference splitting using the approximate Riemann solver developed by Roe.[3] Roe's approximate Riemann solver, combined with the 'Superbee' limiter has been used very successfully to give a second-order method for the Euler equations in one dimension (see References 1 and 4–7). It is found that the first-order part of the method captures shocks crisply over a single cell and the second-order part gives good accuracy in smooth regions, while the use of specific limiters gives sharp contact discontinuities (see References 1 and 5). The scheme is also conservative.

We shall use the similarity of equations (24) and (25) to the Cartesian case to develop a corresponding method for duct flows, keeping as far as possible the above valuable properties.

3.2

We consider a fixed grid in space and time, with grid sizes Δr and Δt respectively, and label the points so that $r_j = r_{j-1} + \Delta r$, $t_n = t_{n-1} + \Delta t$ and $\mathbf{W}_j^n$ and $\mathbf{w}_j^n$ denote the approximations to $\mathbf{W}(r_j, t_n)$ and $\mathbf{w}(r_j, t_n)$ respectively.

Using the relationship $\mathbf{W}(r_j, t_n) = S(r_j)\mathbf{w}(r_j, t_n)$, we may write

$$\mathbf{W}_j^n = \hat{S}_j \mathbf{w}_j^n, \tag{26}$$

where $\hat{S}_j$ represents an average value of $S(r)$. Assuming that at any time $t_n = n\,\Delta t$, $\mathbf{W}_j^n$ represents a piecewise constant approximation to $\mathbf{W}(r_j, t_n)$ in the interval $(r_j - \Delta r/2, r_j + \Delta r/2)$ (as in the usual Godunov approach), $\hat{S}_j$ is given by the volume integral

$$\hat{S}_j = \frac{1}{\Delta r} \int_{r_j - \Delta r/2}^{r_j + \Delta r/2} S(r)\,\mathrm{d}r. \tag{27}$$

(N.B. $\int_{r_j - \Delta r/2}^{r_j + \Delta r/2} S(r)\,\mathrm{d}r$ is the volume of an elemental control volume in the duct.) This enables us to project our initial data $\mathbf{w}(r, 0)$ onto a set of piecewise constant states $\mathbf{W}_j^0$ approximating $\mathbf{W}(r, 0)$, march forward in time and obtain an approximate solution

$$\mathbf{w}_j^n = \mathbf{W}_j^n / \hat{S}_j \tag{28}$$

for $\mathbf{w}(r_j, t_n)$ at time $t = t_n$.

Consider the interval $[r_{j-1}, r_j]$ and denote by $\mathbf{W}_\mathrm{L}$ and $\mathbf{W}_\mathrm{R}$ the approximations to $\mathbf{W}$ at r_{j-1} and r_j respectively. We now rewrite equation (23) as

$$\mathbf{W}_t + \frac{\partial \mathbf{F}(\mathbf{W})}{\partial \mathbf{W}} \mathbf{W}_r = \mathbf{g}(\mathbf{w})$$

and solve approximately the associated Riemann problem

$$\mathbf{W}_t + \tilde{\mathbf{A}}(\mathbf{W}_\mathrm{L}, \mathbf{W}_\mathrm{R})\mathbf{W}_r = \mathbf{g}(\mathbf{w}) \tag{29}$$

with data $\mathbf{W}_\mathrm{L}$ and $\mathbf{W}_\mathrm{R}$ either side of the point $r_{j-1/2}$, linearising by taking $\tilde{\mathbf{A}}(\mathbf{W}_\mathrm{L}, \mathbf{W}_\mathrm{R})$ to be a constant matrix. We shall use a finite difference form of equation (29),

$$\frac{\mathbf{W}_\mathrm{P}^{n+1} - \mathbf{W}_\mathrm{P}^n}{\Delta t} + \tilde{\mathbf{A}}(\mathbf{W}_\mathrm{L}, \mathbf{W}_\mathrm{R}) \frac{\mathbf{W}_j - \mathbf{W}_{j-1}}{\Delta r} = \tilde{\mathbf{g}}(\mathbf{w}^n), \tag{30}$$

where $\tilde{\mathbf{A}}(\mathbf{W}_\mathrm{L}, \mathbf{W}_\mathrm{R})$ is the Roe matrix (31), $\tilde{\mathbf{g}}$ is an approximation to $\mathbf{g}$ and P may be L or R. The Roe matrix $\tilde{\mathbf{A}}(\mathbf{W}_\mathrm{L}, \mathbf{W}_\mathrm{R})$ is an approximation to the Jacobian $\mathbf{A} = \partial \mathbf{F}(\mathbf{W})/\partial \mathbf{W}$ and because of the

remarks following equation (23) it can be seen that

$$\tilde{\mathbf{A}}(\mathbf{W}_L, \mathbf{W}_R) = \tilde{\mathbf{A}}(\mathbf{w}_L, \mathbf{w}_R),$$

where $\tilde{\mathbf{A}}(\mathbf{w}_L, \mathbf{w}_R)$ is an approximation to $\partial \mathbf{f}(\mathbf{w})/\partial \mathbf{w}$. This matrix is constructed so that $\mathbf{f}_R - \mathbf{f}_L = \tilde{\mathbf{A}}(\mathbf{w}_L, \mathbf{w}_R)(\mathbf{w}_R - \mathbf{w}_L)$ for any finite change of state and is given[3] by

$$\tilde{\mathbf{A}} = \begin{bmatrix} 0 & 1 & 0 \\ \frac{\gamma-3}{2}\tilde{U}^2 & (3-\gamma)\tilde{U} & \gamma-1 \\ \frac{\gamma-1}{2}\tilde{U}^2 - \tilde{H}\tilde{U} & \tilde{H} - (\gamma-1)\tilde{U}^2 & \gamma\tilde{U} \end{bmatrix}, \tag{31}$$

where $\tilde{Y}$ denotes a square root mean of left and right states of Y; namely,

$$\tilde{Y} = \frac{\sqrt{\mathscr{R}_L}\, Y_L + \sqrt{\mathscr{R}_R}\, Y_R}{\sqrt{\mathscr{R}_R} + \sqrt{\mathscr{R}_L}} \tag{32}$$

for all variables other than $\mathscr{R}$ and ρ. In later analysis we shall need mean values for $\mathscr{R}$ and ρ, given by

$$\tilde{\mathscr{R}} = \sqrt{(\mathscr{R}_L \mathscr{R}_R)}, \quad \tilde{\rho} = \sqrt{(\rho_L \rho_R)}. \tag{33}$$

The eigenvalues of $\tilde{\mathbf{A}}$ are

$$\tilde{\lambda}_1 = \tilde{U} + \tilde{a}, \quad \tilde{\lambda}_2 = \tilde{U} - \tilde{a}, \quad \tilde{\lambda}_3 = \tilde{U}, \tag{34}$$

with corresponding eigenvectors

$$\tilde{\mathbf{e}}_1 = \begin{pmatrix} 1 \\ \tilde{U} + \tilde{a} \\ \tilde{H} + \tilde{U}\tilde{a} \end{pmatrix}, \quad \tilde{\mathbf{e}}_2 = \begin{pmatrix} 1 \\ \tilde{U} - \tilde{a} \\ \tilde{H} - \tilde{U}\tilde{a} \end{pmatrix}, \quad \tilde{\mathbf{e}}_3 = \begin{pmatrix} 1 \\ \tilde{U} \\ \frac{1}{2}\tilde{U}^2 \end{pmatrix} \tag{35}$$

(as in the standard Cartesian case when $S \equiv 1$), where $\tilde{H}$ is calculated using equation (32) and the mean sound speed $\tilde{a}$ is calculated from

$$\tilde{a}^2 = (\gamma - 1)(\tilde{H} - \tfrac{1}{2}\tilde{U}^2). \tag{36}$$

(N.B. since $|(\tilde{\mathbf{e}}_1, \tilde{\mathbf{e}}_2, \tilde{\mathbf{e}}_3)| = 2\tilde{a}^3/(\gamma - 1)$, the eigenvectors are linearly independent if and only if $\tilde{a} \neq 0$.)

Using the above properties of $\tilde{\mathbf{A}}$, we can write equation (30) in such a way that the left-hand side has its natural conservation form, i.e.,

$$\frac{\mathbf{W}_P^{n+1} - \mathbf{W}_P^n}{\Delta t} + \frac{\mathbf{F}_j - \mathbf{F}_{j-1}}{\Delta r} = \tilde{\mathbf{g}}(\mathbf{w}^n), \tag{37}$$

where $\tilde{\mathbf{g}}(\mathbf{w}^n)$ is a suitable approximation to the term $\mathbf{g}(\mathbf{w})$ on the right-hand side of equation (29). We thus obtain

$$\mathbf{W}_P^{n+1} - \mathbf{W}_P^n = \Delta t \tilde{\mathbf{g}}(\mathbf{w}^n) - (\Delta t/\Delta r)(\mathbf{F}_j - \mathbf{F}_{j-1}). \tag{38}$$

Before we describe the mechanism used to update $\mathbf{W}_j^n$ to $\mathbf{W}_j^{n+1}$, we look at the approximation $\tilde{\mathbf{g}}(\mathbf{w}^n)$ used for $\mathbf{g}(\mathbf{w})$.

Now, $\mathbf{g}(\mathbf{w}) = (0, S'(r)P/S(r), 0)^T$ and we need only to approximate the second component. For this middle component $g_2(\mathbf{w})$ we notice first that, since the sound speed a is given by $a^2 = \gamma p/\rho = \gamma P/\mathscr{R}$,

we may write

$$g_2(\mathbf{w}) = \frac{S'(r)}{S(r)} P = \frac{S'(r)}{S(r)} \frac{\mathscr{R} a^2}{\gamma} = S'(r) \frac{\rho a^2}{\gamma}.$$

The reason for doing this is that $g_2(\mathbf{w})$ now has a more 'natural' approximation in the framework we have set up in the sense that $\hat{S}$ is averaged in the same may as $\mathscr{R}$; i.e.,

$$\tilde{g}_2(\mathbf{w}^n) = \frac{\hat{S}_j - \hat{S}_{j-1}}{\Delta r} \frac{\tilde{\rho} \tilde{a}^2}{\gamma}, \tag{39}$$

where $\tilde{a}^2$ is as before and

$$\tilde{\rho} = \sqrt{(\rho_L \rho_R)} = \frac{\sqrt{(\mathscr{R}_L \mathscr{R}_R)}}{\sqrt{(\hat{S}_L \hat{S}_R)}} = \frac{\tilde{\mathscr{R}}}{\tilde{S}}$$

In the homogeneous case, the procedure now[3] is to project $\Delta \mathbf{f} = \mathbf{f}_j - \mathbf{f}_{j-1}$ onto the eigenvectors of $\tilde{\mathbf{A}}$. Each projection represents the contribution of one wave system to $\Delta \mathbf{f}$. Here we follow a suggestion of Roe[8] and find the projections both of $\Delta \mathbf{f} = \mathbf{F}_j - \mathbf{F}_{j-1}$ and also $\tilde{\mathbf{g}}(\mathbf{w}^n)$. Roe shows that for linear conservation laws this procedure leads to a correctly 'upwinded' treatment of source terms. We then update $\mathbf{W}_j^n$ to $\mathbf{W}_j^{n+1}$ as follows. Suppose that we can find wave speeds $\tilde{\lambda}_i$ and wave strengths $\tilde{\alpha}_i$ such that

$$\Delta_r \mathbf{W} = \mathbf{W}_j - \mathbf{W}_{j-1} = \sum_{i=1}^{3} \tilde{\alpha}_i \tilde{\mathbf{e}}_i \tag{40}$$

and

$$\Delta_r \mathbf{F} = \sum_{i=1}^{3} \tilde{\alpha}_i \tilde{\lambda}_i \tilde{\mathbf{e}}_i. \tag{41}$$

Since $\tilde{\mathbf{A}}$ has eigenvalues $\tilde{\lambda}_i$ with corresponding eigenvectors $\tilde{\mathbf{e}}_i$, and we may also expand the source term $\tilde{\mathbf{g}}(\mathbf{w}^n)$ in terms of the $\tilde{\mathbf{e}}_i$ as, say,

$$\tilde{\mathbf{g}}(\mathbf{w}^n) = -\frac{1}{\Delta r} \sum_{i=1}^{3} \tilde{\beta}_i \tilde{\mathbf{e}}_i, \tag{42}$$

we may write equations (37) as

$$\mathbf{W}_P^{n+1} = \mathbf{W}_P^n - \frac{\Delta t}{\Delta r} \sum_{i=1}^{3} \tilde{\lambda}_i \tilde{\gamma}_i \tilde{\mathbf{e}}_i, \tag{43}$$

where

$$\tilde{\gamma}_i = \tilde{\alpha}_i + \tilde{\beta}_i / \tilde{\lambda}_i \tag{44}$$

and P may be L or R depending on the sign of $\tilde{\lambda}_i$.

If we follow the algebra through, we obtain for the $\tilde{\alpha}_i$ in (40) and (41)

$$\tilde{\alpha}_1 = \frac{1}{2\tilde{a}^2} (\Delta_r P + \tilde{\mathscr{R}} \tilde{a} \Delta_r U), \quad \tilde{\alpha}_2 = \frac{1}{2\tilde{a}^2} (\Delta_r P - \tilde{\mathscr{R}} \tilde{a} \Delta_r U), \quad \tilde{\alpha}_3 = \Delta_r \mathscr{R} - \frac{\Delta_r P}{\tilde{a}^2} \tag{45a}$$

and for the $\tilde{\beta}_i$ in (42)

$$\tilde{\beta}_1 = \frac{\tilde{\mathscr{R}} \Delta_r \hat{S}}{2\gamma \tilde{S}} [(\gamma - 1)\tilde{U} - \tilde{a}], \quad \tilde{\beta}_2 = \frac{\tilde{\mathscr{R}} \Delta_r \hat{S}}{2\gamma \tilde{S}} [(\gamma - 1)\tilde{U} + \tilde{a}], \quad \tilde{\beta}_3 = -\frac{(\gamma - 1)\tilde{\mathscr{R}} \tilde{U} \Delta_r \hat{S}}{\gamma \tilde{S}}. \tag{45b}$$

(Note that the quantity $\Delta_r \hat{S} / \tilde{S}$ is independent of time and therefore has to be calculated only once. If

the area changes are due to central symmetry, so that $S(r) = kr^{\sigma}$, where $\sigma = 1, 2$ for cylindrical or spherical flow, then

$$\frac{\Delta_r \hat{S}}{\tilde{S}} = \frac{r_j - r_{j-1}}{(r_j r_{j-1})^{1/2}} \quad \text{if} \quad \sigma = 1$$

and

$$\frac{\Delta_r \hat{S}}{\tilde{S}} = \frac{r_j^2 - r_{j-1}^2}{r_j r_{j-1}} \quad \text{if} \quad \sigma = 2.$$

Since these expressions are singular when a grid point is placed at the origin, we use grids that straddle the origin.)

The expressions in equations (45a, b) have been written in terms of primitive variables for simplicity. The expressions for $\tilde{\alpha}_1, \tilde{\alpha}_2$ and $\tilde{\alpha}_3$ follow those given by Roe and Pike[4] and signify wave strengths which would be generated by the data $[\mathbf{W}_{j-1}, \mathbf{W}_j]$ in a parallel duct. The expressions for $\tilde{\beta}_1, \tilde{\beta}_2$ and $\tilde{\beta}_3$ represent modifications to those wave strengths due to area changes. The following identities are useful in deriving equations (45a, b):

$$\Delta_r(\mathscr{R}U) = \tilde{\mathscr{R}}\,\Delta_r U + \tilde{U}\,\Delta_r \mathscr{R}, \quad \Delta_r(\mathscr{R}U^2) = \tilde{U}^2\,\Delta r \mathscr{R} + 2\tilde{\mathscr{R}}\tilde{U}\,\Delta_r U.$$

We also note another identity, namely,

$$\tilde{a}^2 = \frac{\gamma[\sqrt{\mathscr{R}_L}(P_L/\mathscr{R}_L) + \sqrt{\mathscr{R}_R}(P_R/\mathscr{R}_R)]}{\sqrt{\mathscr{R}_L} + \sqrt{\mathscr{R}_R}} + \frac{(\gamma - 1)\tilde{\mathscr{R}}(\Delta U)^2}{2(\sqrt{\mathscr{R}_L} + \sqrt{\mathscr{R}_R})^2}, \tag{46}$$

which ensures that $\tilde{a}^2$ is non-negative for real data. Moreover, it gives conditions for the local sound speed to vanish; namely, $P_L = P_R = 0$, $\Delta_r U = 0$; i.e., $p_L = p_R = 0$, $u_L = u_R$. This corresponds to special data for which both the wave speeds $\tilde{U}$ and eigenvectors $(1, \tilde{U}, \frac{1}{2}\tilde{U}^2)^T$ are equal, so that in this case the scheme reduces to

$$\mathbf{W}_P^{n+1} - \mathbf{W}_P^n + \frac{\Delta t}{\Delta r}\tilde{U}\,\Delta_r \mathscr{R} \begin{pmatrix} 1 \\ \tilde{U} \\ \frac{1}{2}\tilde{U}^2 \end{pmatrix} = \mathbf{0}, \tag{47}$$

representing an advancement of $\mathbf{W}_P^n$ entirely due to changes in the density profile. Although computationally this case would appear to be difficult to handle, we notice that, when $\tilde{a} = 0$, by changing $\tilde{a}^2$ to a non-zero value the scheme reproduces equations (47). (The non-Cartesian geometry is still present since $\mathbf{W} = S(r)\mathbf{w}$.)

To solve equations (24) and (25) using the finite difference approximation given by equations (43) and (44), we use the method of upwind differencing on the three waves with wave speeds $\tilde{\lambda}_1, \tilde{\lambda}_2$ and $\tilde{\lambda}_3$ and wave strengths $\tilde{\gamma}_1, \tilde{\gamma}_2, \tilde{\gamma}_3$ (which will differ from the usual wave strengths in slab symmetry due to the variation of $S(r)$).

To update $\mathbf{W}^n$ to $\mathbf{W}^{n+1}$, we use first-order upwind differencing; i.e., for each cell $[r_{j-1}, r_j]$ we add $-(\Delta t/\Delta r)\tilde{\lambda}_i\tilde{\gamma}_i\tilde{\mathbf{e}}_i$ to $\mathbf{W}_j^n$ when $\tilde{\lambda}_i > 0$ and add $-(\Delta t/\Delta r)\tilde{\lambda}_i\tilde{\gamma}_i\tilde{\mathbf{e}}_i$ to $\mathbf{W}_{j-1}^n$ when $\tilde{\lambda}_i < 0$ (see Figure 1). This gives a first-order approximation and exact shock recognition for the Riemman problem given by equation (29) within the resolution of the grid, provided that we use the previously defined local averages given by equations (32) and (33) (see Reference 3).

We can now calculate second-order corrections by transferring fractions of the increments described in Figure 1. If we 'limit' these transfers using a suitable flux limiter or B function (see References 1, 4 and 5), the scalar scheme will be second-order almost everywhere, oscillation-free and will sharpen up certain features that will be smeared by using the first-order method only. In

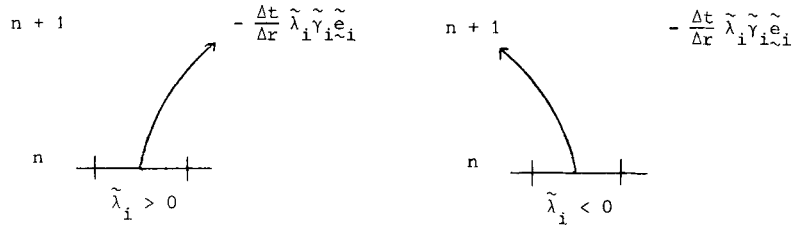

Figure 1. Schematic representation of the first-order algorithm

addition, a device may be incorporated into the scheme to disperse entropy-violating solutions and treat expansion fans correctly (see Reference 9).

In the next section we note the properties of the scheme described above in relation to the type of problem we wish to solve.

4. PROPERTIES OF THE SCHEME

In this section we discuss briefly some properties of the scheme proposed here for solving equations (17)–(20) in relation to the features that we expect to occur in this type of problem.

(i) The scheme is 'conservative' in the following sense. Equations (17) and (19) represent conservation of mass, $\int \rho S(r)\,dr$, and energy, $\int eS(r)\,dr$, but conservation of momentum, $\int \rho uS(r)\,dr$, is not maintained in equation (18). This is because the pressure term arises as $S(r)p_r$ which is not derivable from a potential. However, $[S(r)p]_r$ is derivable from a potential, but leads to a non-zero right-hand side term $S'(r)p$ (since in the non-Cartesian case $S \not\equiv 1$). Thus integrating equation (23) gives

$$\frac{\partial}{\partial t}\left(\int_{r_{j-1}}^{r_j} \mathbf{W}\,dr\right) = -\mathbf{F}(\mathbf{W})\Big|_{r_{j-1}}^{r_j} + \begin{pmatrix} 0 \\ \int_{r_{j-1}}^{r_j} S'(r)p\,dr \\ 0 \end{pmatrix}. \tag{48}$$

Therefore, in the region $0 \leqslant r \leqslant 1$,

$$\frac{\partial}{\partial t}\left(\int_0^1 \mathbf{W}\,dr\right) = -(\mathbf{F}_1 - \mathbf{F}_0) + \begin{pmatrix} 0 \\ \int_0^1 S'(r)p\,dr \\ 0 \end{pmatrix}. \tag{49}$$

Thus the first and last components of $\mathbf{W}$ are conserved and, if $S'(r) \equiv 0$, so is the middle component.

We now show that the scheme given by equations (43) and (44) is also 'conservative' in a finite difference sense. Since by construction $\tilde{\mathbf{A}}\,\Delta_r\mathbf{W} = \Delta_r\mathbf{F}$, we have

$$\mathbf{W}_j^{n+1} = \mathbf{W}_j^n - \frac{\Delta t}{\Delta r}\Delta_r\mathbf{F} + \Delta t\begin{pmatrix} 0 \\ \tilde{g}_2(\mathbf{w}^n) \\ 0 \end{pmatrix}. \tag{50}$$

Thus

$$\sum_j \mathbf{W}_j^{n+1} = \sum_j \mathbf{W}_j^n - \frac{\Delta t}{\Delta r}(\mathbf{F}_N - \mathbf{F}_0) + \begin{pmatrix} 0 \\ \Delta t \sum_j \tilde{g}_2(\mathbf{w}^n) \\ 0 \end{pmatrix}, \tag{51}$$

where $N\,\Delta r = 1$. Thus the finite difference scheme is again 'conservative', in the sense that the first and last components of $\mathbf{W}^n$ are conserved, and the second component will be conserved if $S'(r) \equiv 0$; i.e., $\Delta_r \hat{S} = 0$; i.e., $\tilde{g}_2(\mathbf{w}^n) = 0$.

(ii) If we consider the special case of constant data $\rho_j^n = \rho^n$, $u_j^n = u^n$, $p_j^n = p^n$ for all j at time $t = n\,\Delta t$, equations (43) and (44) reduce to

$$\frac{\mathbf{W}_j^{n+1} - \mathbf{W}_j^n}{\Delta t} + \frac{\Delta_r \hat{S}}{\Delta r} \begin{pmatrix} \rho^n u^n \\ \rho^n (u^n)^2 \\ u^n (e^n + p^n) \end{pmatrix} = 0, \tag{52}$$

giving a direct finite difference analogue of equations (21) and (22) with $\mathbf{u}_r = \mathbf{0}$ (corresponding to $\Delta_r \mathbf{u} = 0$). Equations (52) have the solution

$$\rho_j^{n+k} = \rho^n \left(1 - \frac{\Delta t u^n \Delta_r \hat{S}}{\Delta r \tilde{S}}\right) \tag{53a}$$

$$u_j^{n+k} = u^n, \tag{53b}$$

$$p_j^{n+k} = p^n \left(1 - \frac{\Delta t \gamma u^n \Delta_r \hat{S}}{\Delta r \tilde{S}}\right)^k \tag{53c}$$

for $k \geqslant 0$, which are approximate solutions to the exact solutions of equations (21) and (22) with this given data; namely,

$$\rho(j\,\Delta r, (n+k)\,\Delta t) = \rho^n \mathrm{e}^{-k\Delta t u^n [S'(r)/S(r)]}, \tag{54a}$$

$$u(j\,\nabla r, (n+k)\,\Delta t) = u^n, \tag{54b}$$

$$p(j\Delta r, (n+k)\,\Delta t) = p^n \mathrm{e}^{-k\Delta t \gamma u^n [S'(r)/S(r)]}. \tag{54c}$$

In particular, with $u^n = 0$ (no flow) and constant density and pressure, ρ^n and p^n respectively, equations (53a–c) yield the correct physical solution; namely, $u^{n+k} = 0$, $\rho^{n+k} = \rho^n$, $p^{n+k} = p^n$.

(iii) The scheme 'recognizes' steady states. If the data satisfies the compact residual equation

$$\mathbf{F}_j - \mathbf{F}_{j-1} = \Delta r\, \tilde{g}(\mathbf{w})_{j-1/2} \quad \text{for all } j, \tag{55}$$

then $\tilde{\lambda}_1 = \tilde{\lambda}_2 = \tilde{\lambda}_3 = 0$ for all pairs of cells and no updating takes place. Equation (55) can be regarded as a two-point discretization, second-order accurate at $r_{j-1/2}$ of the ordinary differential equations governing steady compressible flow. This property appears especially valuable when shock reflection should leave behind a uniform unchanging flow, as in Problem 1 in §5.

(iv) The scheme also 'recognizes' shock waves. At a shock, $\Delta_r \mathbf{F} = s\,\Delta_r \mathbf{W}$ for some scalar shock speed s and, by equations (40) and (41), s is an eigenvalue of $\tilde{\mathbf{A}}$. The projection of $\Delta_r \mathbf{W}$ onto the local eigenvectors of $\tilde{\mathbf{A}}$ will be solely onto the eigenvector which corresponds to s. In this special case, the solution of the linearized Riemann problem given by equation (40) is exact (see Reference 3 and below).

The reason that the formulation (40) recognizes shocks is that the right-hand side term $\mathbf{g}(\mathbf{w})$ does not contribute to the shock wave, essentially because it does not contain any derivatives in $\mathbf{w}$, and therefore no jumps. In particular, suppose that the pressure p jumps from p_L to p_R at $r = r_0$; then

$$\lim_{\varepsilon \to 0} \int_{r_0-\varepsilon}^{r_0+\varepsilon} S'(r) \mathrm{p}\, \mathrm{d}r = \lim_{\varepsilon \to 0} \{p_L[S(r_0) - S(r_0 - \varepsilon)] + p_R[S(r_0 + \varepsilon) - S(r_0)]\} = 0,$$

since $S(r)$ is continuous. Thus

$$\lim_{\varepsilon \to 0} \int_{r_0-\varepsilon}^{r_0+\varepsilon} \mathbf{g}(\mathbf{w})\, \mathrm{d}r = \mathbf{0}; \tag{56}$$

i.e., the shock speed is given by $\Delta_r \mathbf{F}(\mathbf{W})/\Delta_r \mathbf{W}$, with the right-hand side making no contribution.

Moreover, in terms of the three scalar problems obtained by diagonalizing the system given by equation (30) with $\mathbf{A}$ a constant matrix, we have

$$\frac{\partial v_i}{\partial t} + \lambda_i \frac{\partial v_i}{\partial r} = h_i(\mathbf{w}), \quad i = 1, 2, 3, \tag{57}$$

where

$$\mathbf{v} = \mathbf{X}^{-1}\mathbf{w}, \quad \mathbf{h} = \mathbf{X}^{-1}\mathbf{g}$$

and $\mathbf{X}$ is the modal matrix consisting of the eigenvectors of $\mathbf{A}$ with eigenvalues λ_i. Solutions to equation (57) can be represented in terms of a 'shock solution', this being a solution of the homogeneous equation—i.e., equation (57) with $\mathbf{h}(\mathbf{w}) = \mathbf{0}$—and a 'source solution', this being the particular solution of the inhomogeneous equation (57). In effect, the scheme we have developed solves equation (57) approximately, and thus the important 'shock solution' is modelled as a consequence of the construction of $\tilde{\mathbf{A}}$.

In the next section we discuss two test problems that can be used to test algorithms for solving equations (17)–(20).

5. TEST PROBLEMS

In this section we look at two test problems used to test the previously described algorithm for solving equations (17)–(20).

Problem 1

The first problem, proposed by Noh,[10] is concerned with infinite shock reflection and can be posed in slab, cylindrical or spherical symmetry, denoted by $d = 1, 2$ or 3 respectively.

We consider a region $0 \leqslant r \leqslant 1$ with initial conditions

$$\rho(r, 0) = 1, \quad u(r, 0) = -1, \quad p(r, 0) = 0;$$

i.e., low-energy gas (zero temperature) moving towards $r = 0$. This represents shock reflection from a rigid wall ($d = 1$), an axis of symmetry ($d = 2$) or the centre of a sphere ($d = 3$), all at $r = 0$. The gas is brought to rest at $r = 0$, and denoting (0) initial values, $(-)$ pre-shocked values and $(+)$ post-shocked values, we have the exact solution (see Reference 10)

$$\rho^0 = 1, \quad \rho^- = \left(\frac{\gamma+1}{\gamma-1}\right)^{d-1} \rho^0, \quad \rho^+ = \left(\frac{\gamma+1}{\gamma-1}\right)\rho^-, \tag{58a}$$

$$u^0 = -1, \quad u^- = -1, \quad u^+ = 0, \tag{58b}$$

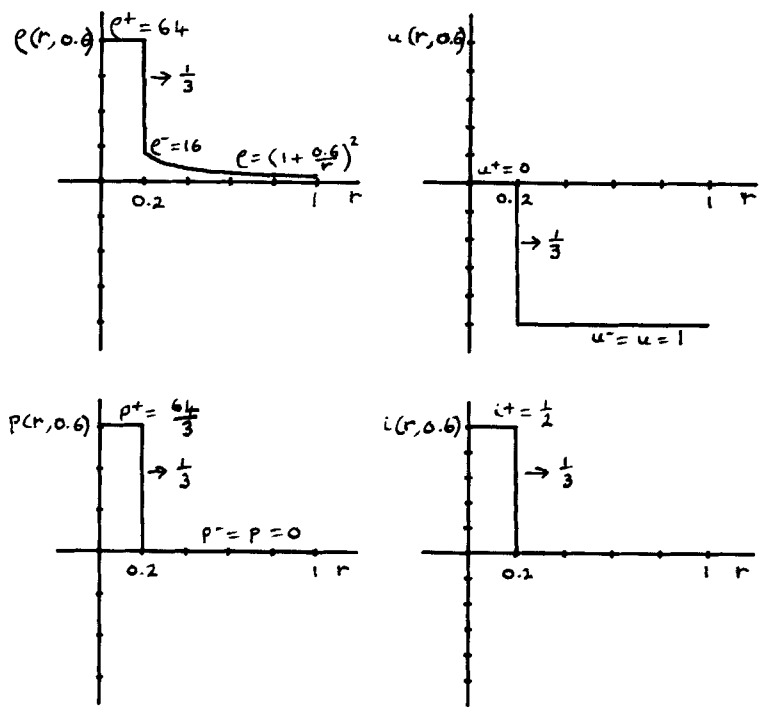

Figure 2. The exact solution of Problem 1 with $d = 3$, $\gamma = 5/3$ at $t = 0{\cdot}6$

$$p^0 = 0, \quad p^- = 0, \quad p^+ = \frac{\gamma - 1}{2}\rho^+ \tag{58c}$$

and

$$\rho = \left(1 + \frac{t}{r}\right)^{d-1}, \quad u = -1, \quad p = 0 \quad \text{for } \frac{r}{t} \geqslant \frac{\gamma - 1}{2}. \tag{58d}$$

The shock moves out from the origin with speed $(\gamma - 1)/2$. (N.B. $p^+/p^- = \infty$.)

Taking the spherical case as an example, with $d = 3$ and $\gamma = 5/3$ (a monoatomic gas), the exact solution at $t = 0{\cdot}6$ is shown in Figure 2.

The case $d = 1$ is a standard test problem in shock reflection and the solution is not difficult to compute. However, the cases $d = 2$ and $d = 3$ are much more difficult to model (see Noh[10]).

It is the last case, $d = 3$, that we concentrate on here; i.e., a spherically infinite diverging shock, for various values of γ. (N.B. Here $S(r) = r^2$.)

Problem 2

The second test problem is concerned with a converging cylindrical shock. Here we consider a region $0 \leqslant r \leqslant 200$ for the cylindrically symmetric case given by equations (17)–(20) with $S(r) = r$.

Initially, a cylindrical diaphragm of radius $r = 100$ separates two uniform regions of an ideal gas at rest ($\gamma = 1{\cdot}4$, a diatomic gas; e.g., air). The initial conditions are $p = \rho = 4$ in the outer region and $p = \rho = 1$ in the inner region. When the diaphragm is removed at $t = 0$, a converging shock wave followed by a converging contact discontinuity move towards the axis, $r = 0$, and a diverging rarefaction wave moves outwards.

The shock accelerates as it approaches the axis of symmetry, is reflected from the axis and interacts with the contact discontinuity (still converging), which results in a transmitted shock, a converging contact discontinuity and a weak converging reflected shock. This problem has been treated by Ben-Artzi and Falcovitz[11] using a more complicated Riemman solver. In the next section we display numerical results for the two problems described above.

6. NUMERICAL RESULTS

In this section we exhibit numerical results obtained for the two test problems described in §5 using the scheme described in §3. In both cases we apply a reflection condition at $r = 0$; i.e., we add an 'image' cell at the boundary $r = 0$ and impose equal density and pressure, and equal and opposite velocity, at either end of the cell. This results in no net movement in the cell. Two 'image' cells are required for the second-order method.

Problem 1

Figures 3–5 refer to Problem 1 using either the first-order scheme or the second-order scheme with the Superbee limiter (see References 1 and 5). We vary the output times, but the number of mesh points remains fixed at 100.

We note that, because the incoming flow at $r = 1$ is supersonic, we have imposed the exact solution there: however, this condition can easily be replaced by introducing a low-energy gas at the right-hand end.

Problem 2

Figures 6–11 refer to Problem 2 using the second-order scheme with the Superbee limiter. We have used $\gamma = 1{\cdot}4$ and 200 mesh points.

For Problem 1 we note the extremely good representation of the solution and propagation of the shock in time. Although it is a simple test problem, it has been found difficult to achieve good results (see Noh[10]). Since the only feature in the solution is a shock discontinuity, the first-order method works well, with a slight lack of resolution in the smooth part of the flow.

For Problem 2 we have found that the first-order method is not as accurate since the solution has a number of features that require good resolution. However, the second-order scheme applied with the Superbee limiter compares well with the solutions computed by Ben-Artzi and Falcovitz,[11] especially in the weak converging shock present at $t = 110$.

For both problems we see that the discontinuities move with the correct speed. This feature is a consequence of writing the equations in 'conservation' form and of using the Roe averaging for the new variables. The use of flux limiters sharpens up these features without introducing non-physical oscillations. Furthermore, upwinding the source terms after projecting them onto the local eigenvectors leads to the correct treatment of the linearized equations (see Reference 8).

The CPU time required to compute the results on an Amdahl V/7A was found to be as follows:

(i) Problem 1 with Superbee and 100 mesh points takes 0·0157 CPU seconds to compute one time step and a total of 1·256 CPU seconds to reach a real time of 0·6 using 80 time steps.

(ii) Problem 2 with Superbee and 200 mesh points takes 0·04 CPU seconds to compute one time step and a total of 8·64 CPU seconds to reach a real time of 54 using 216 time steps. The reason for the amount of CPU time used per time step per mesh point being higher in Problem 2 is that we needed to include the entropy modification mentioned in §3.

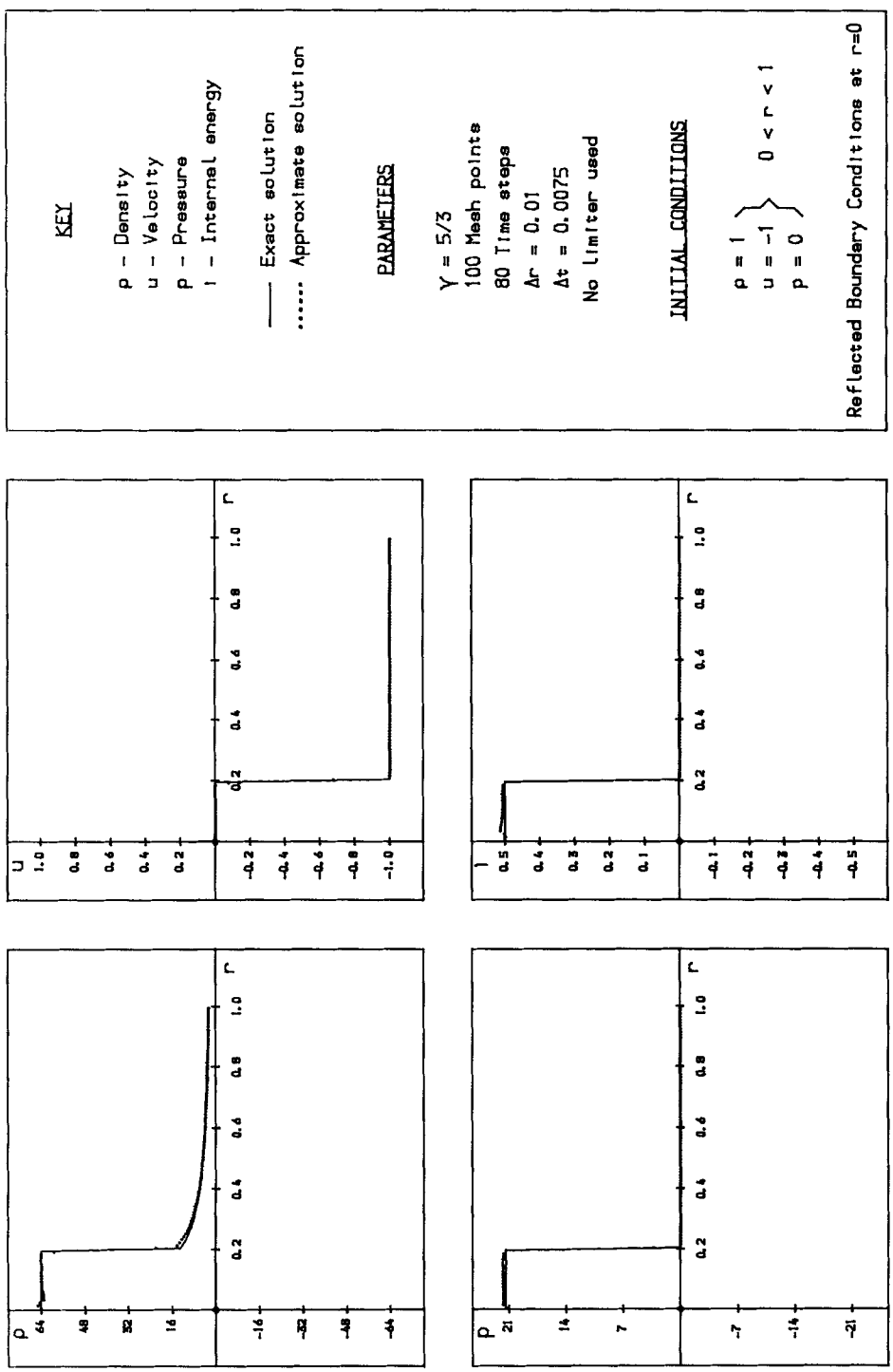

Figure 3. Results for Problem 1 with $\gamma = 5/3$ using the first-order scheme at $t = 0{\cdot}6$

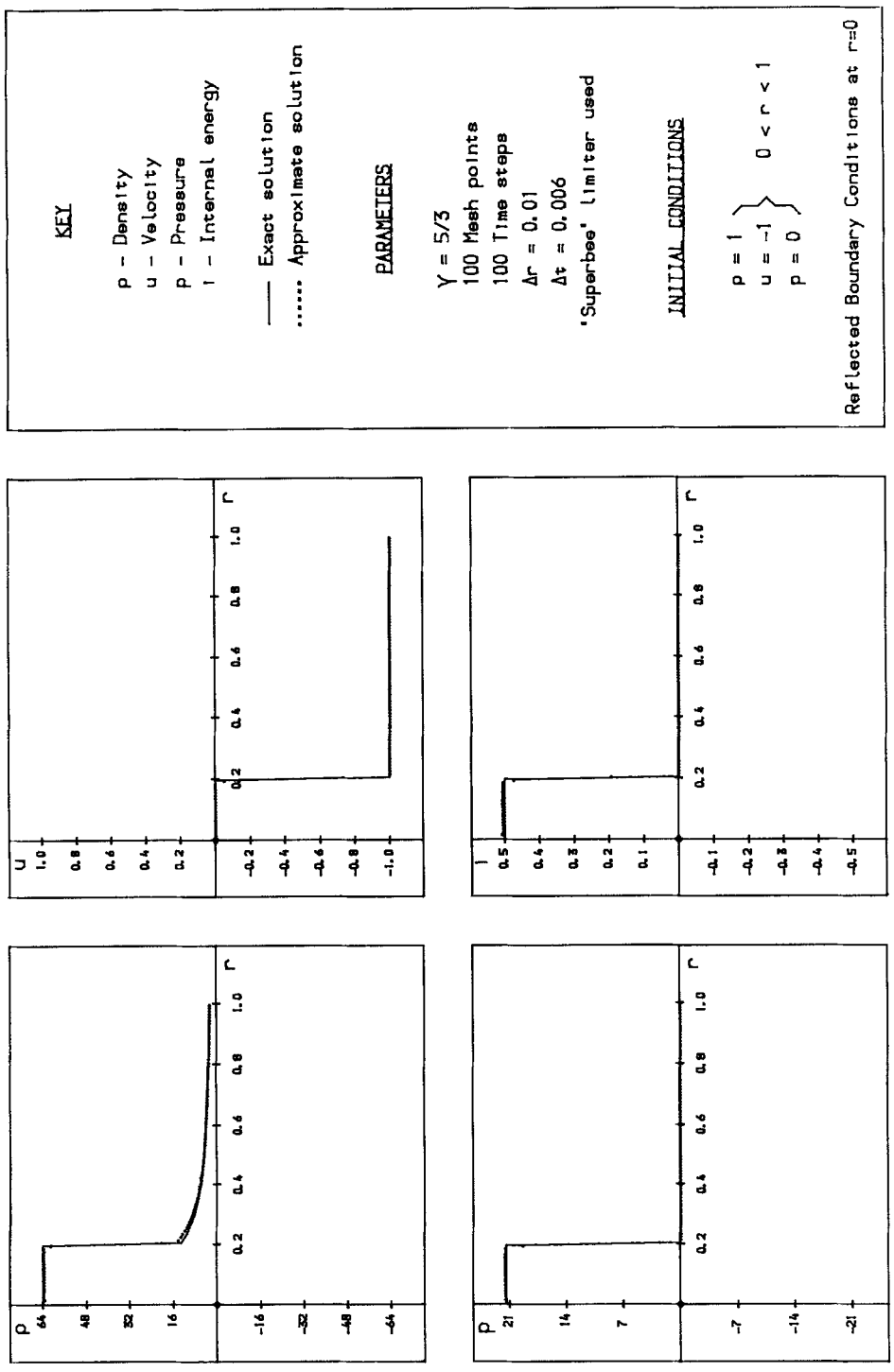

Figure 4. Results for Problem 1 with $\gamma = 5/3$ using the second-order scheme with the Superbee limiter at $t = 0.6$

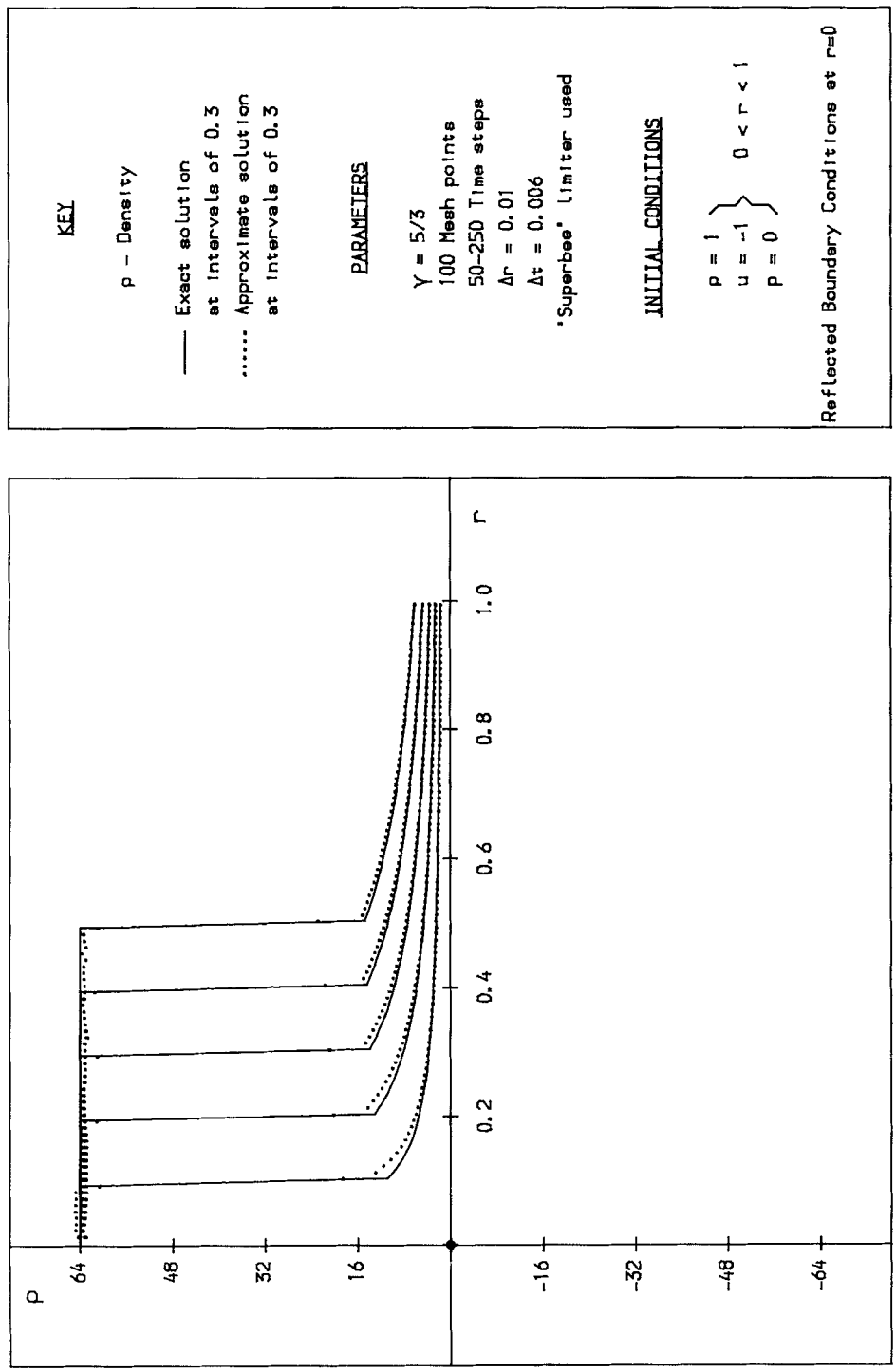

Figure 5. Results for Problem 1 with $\gamma = 5/3$ using the second-order scheme with the Superbee limiter at $t = 0{\cdot}3, 0{\cdot}6, 0{\cdot}9, 1{\cdot}2, 1{\cdot}5$

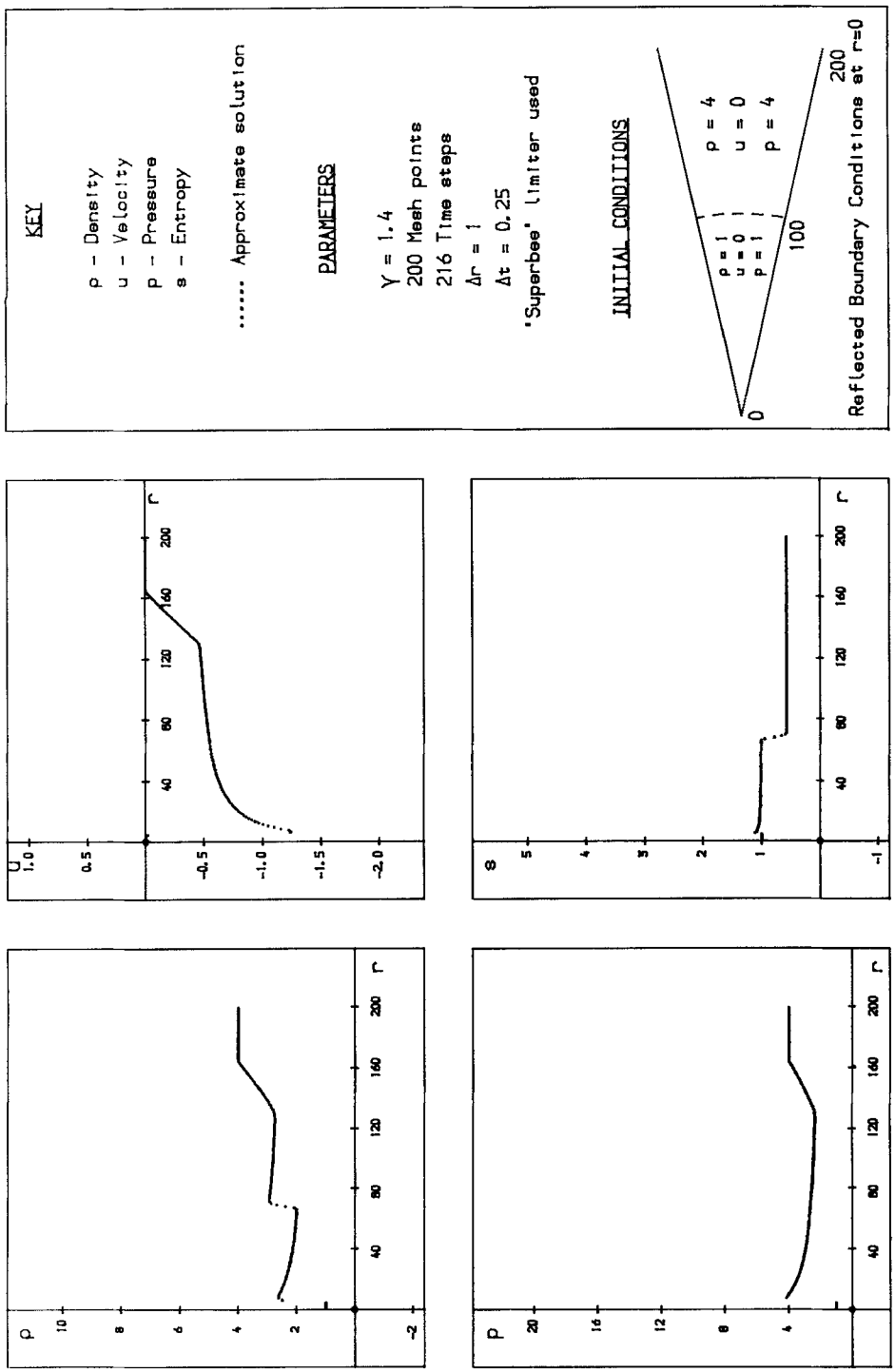

Figure 6. Results for Problem 2 at $t = 54$. The converging shock approaches $r = 0$

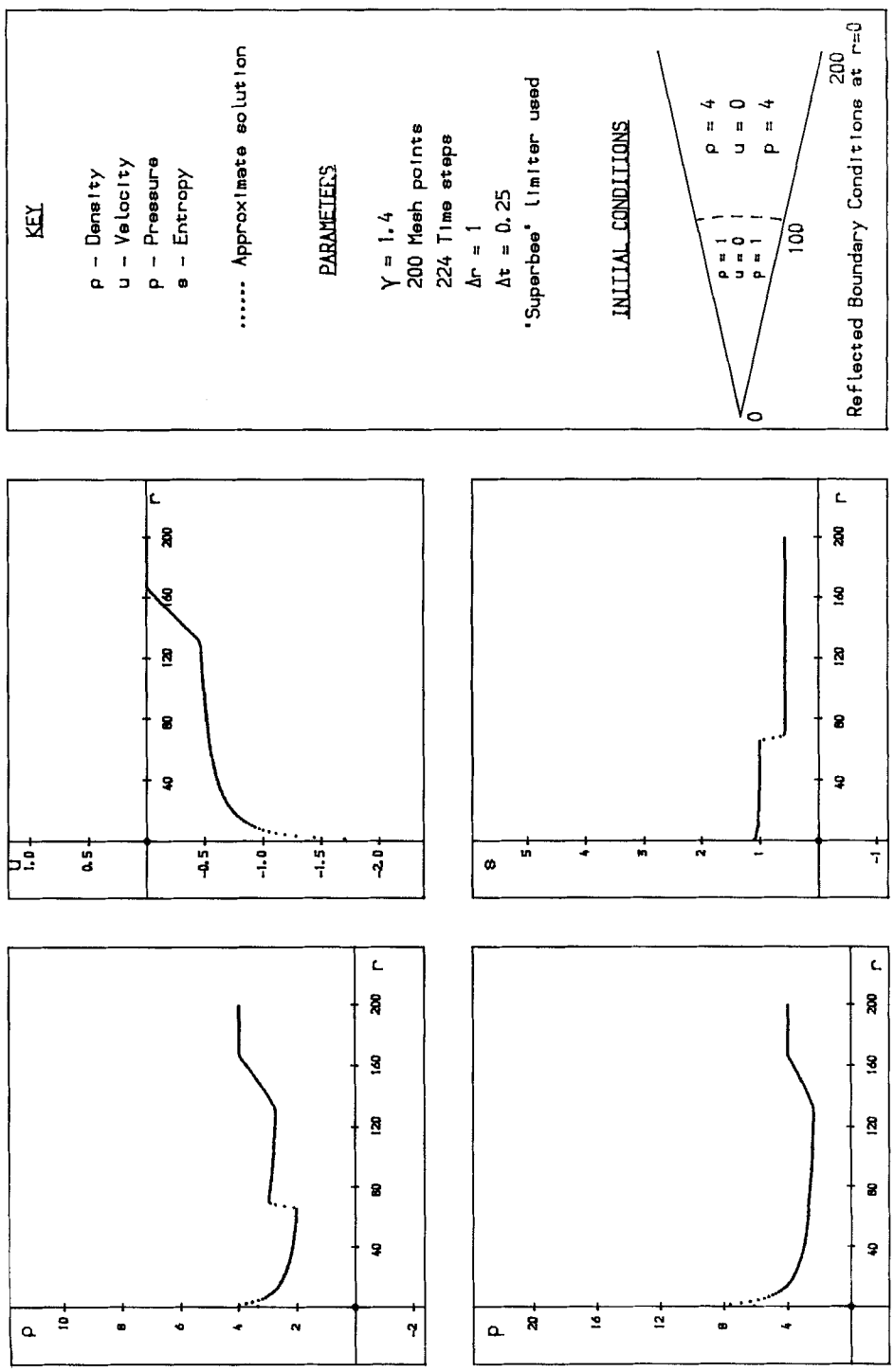

Figure 7. Results for Problem 2 at $t = 56$. The shock is about to hit the axis

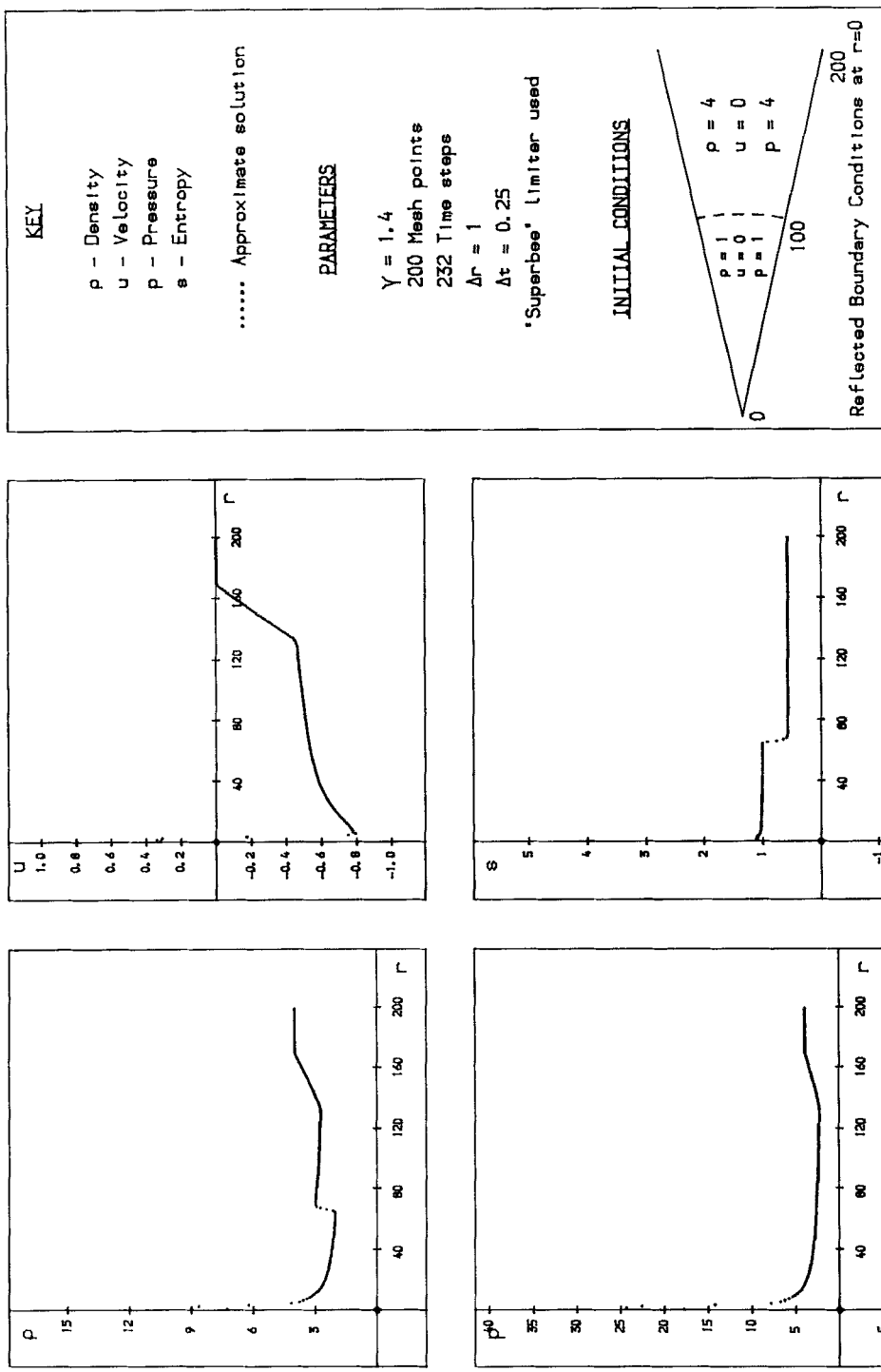

Figure 8. Results for Problem 2 at $t = 58$. The shock has been reflected from the axis

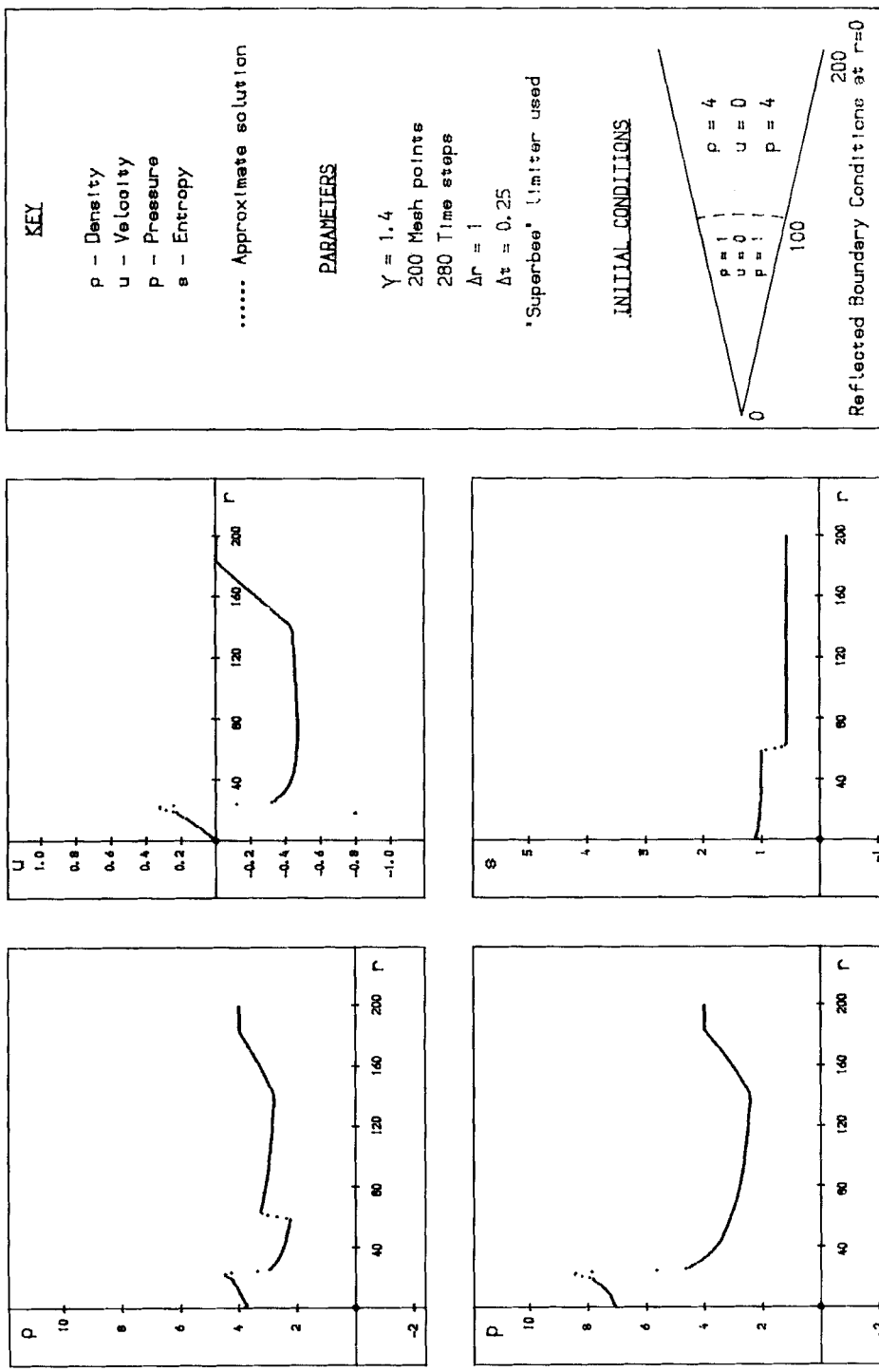

Figure 9. Results for Problem 2 at $t = 70$. The diverging shock (followed by a rarefaction wave) is heading towards the converging contact discontinuity

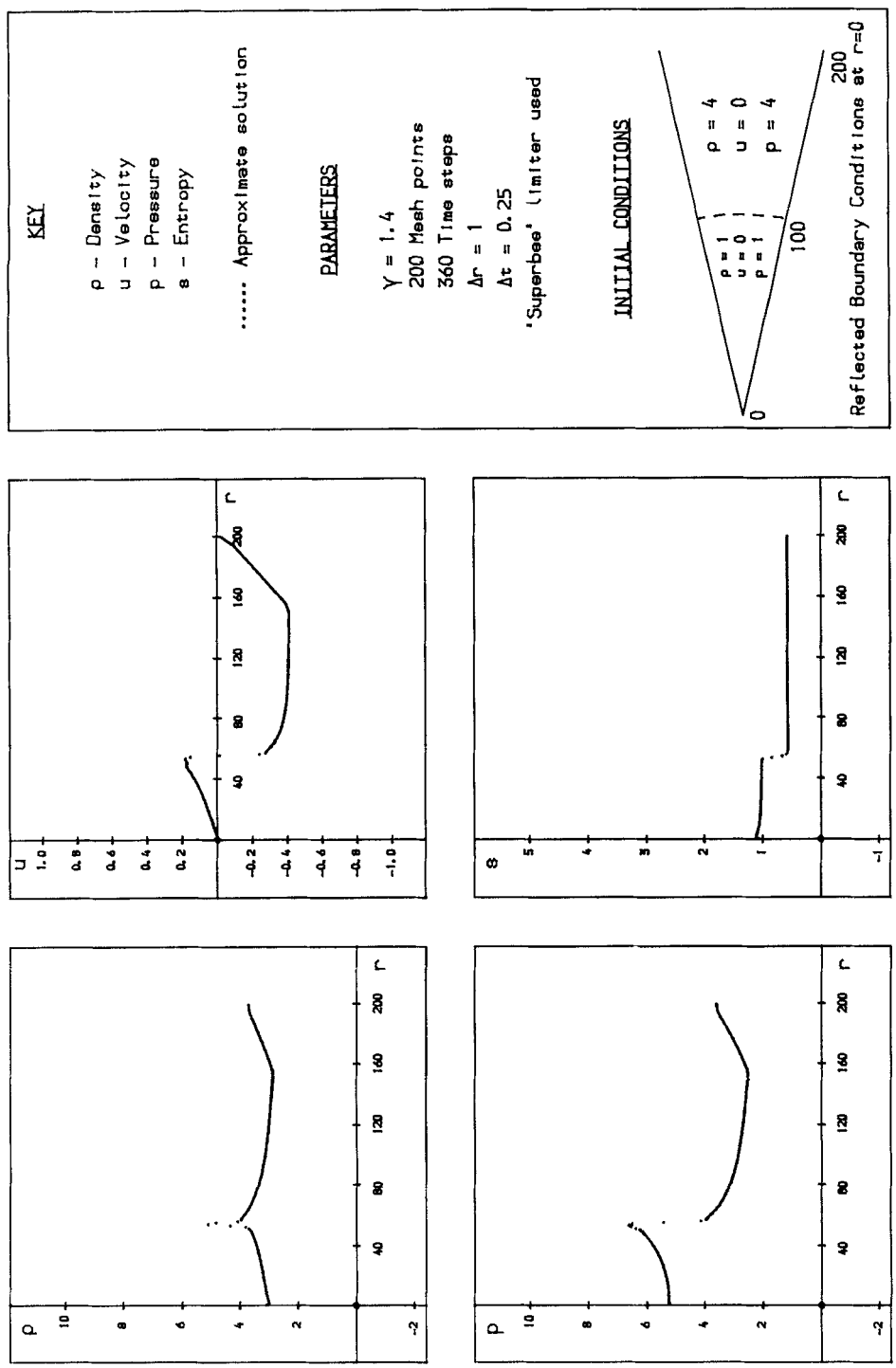

Figure 10. Results for Problem 2 at $t = 90$. The interaction of the shock and contact discontinuity

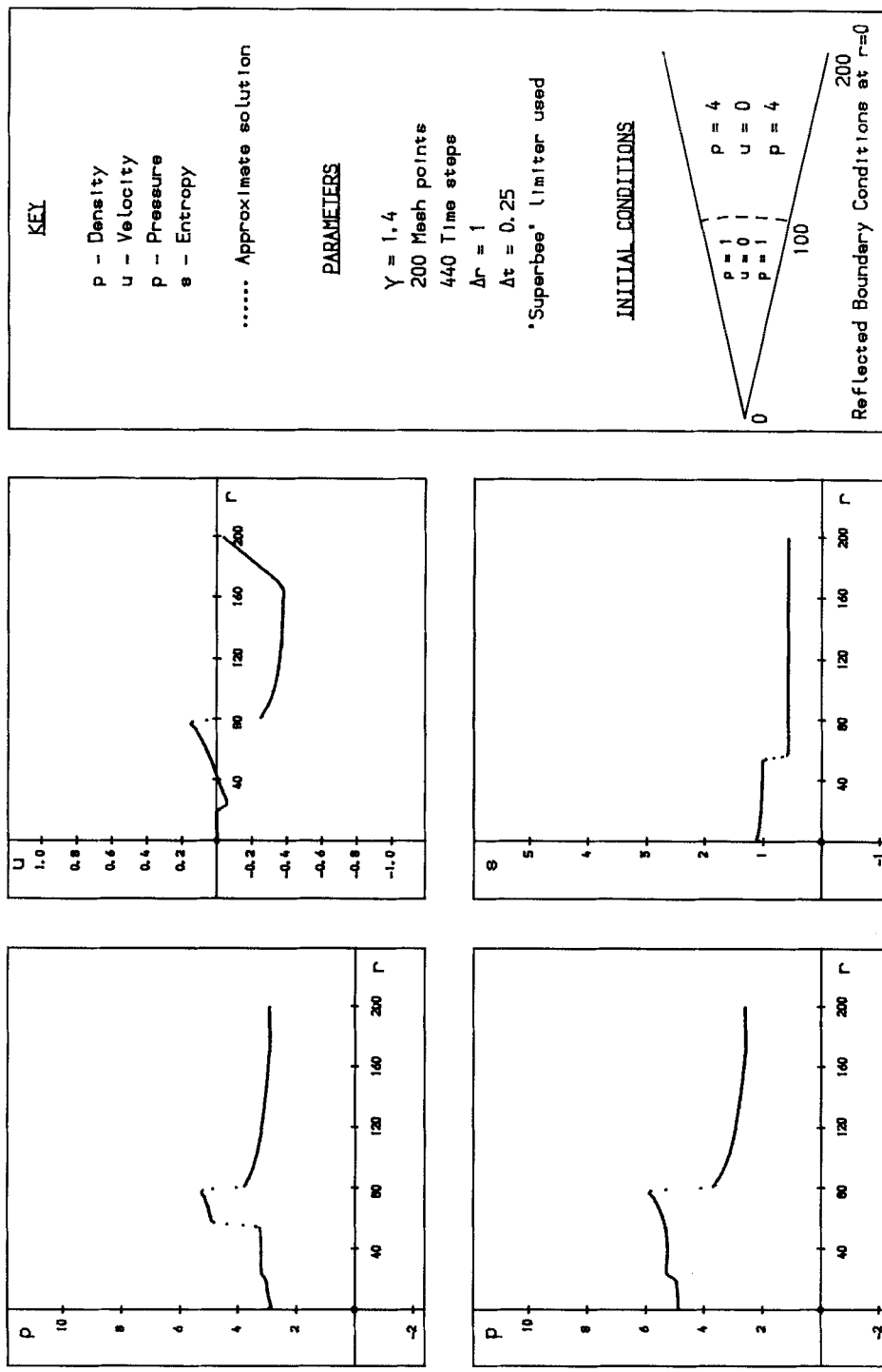

Figure 11. Results for Problem 2 at $t = 110$. The interaction results in a diverging transmitted shock, a converging contact discontinuity and a weak converging shock

A minor modification to our algorithm allows for a variable (adaptive) time step and gives the ability to decrease the total amount of computing time used.

7. CONCLUSIONS

We have extended the one-dimensional version of Roe's scheme to include cylindrically and spherically symmetric problems. We have shown how these problems break away from standard 'conservation' form and thus give rise to source terms, and that with the approach outlined in §3 we can achieve good results on standard test problems. In particular, by writing the equations in a special form, using the Roe averaging, and upwinding the projected source terms, we obtain the correct speed for shock and contact discontinuities. Moreover, the algorithm is computationally efficient.

ACKNOWLEDGEMENTS

I would like to express my thanks to Dr. M. J. Baines for many useful discussions and to Professor P. L. Roe for a number of invaluable suggestions.

This work forms part of the research programme of the Institute for Computational Fluid Dynamics at the Universities of Oxford and Reading and was funded by AWRE, Aldermaston under contract No. NSN/13B/2A88719.

REFERENCES

1. P. L. Roe, 'Some contributions to the modelling of discontinuous flows', *Proc. AMS/SIAM Seminar*, San Diego, 1983.
2. A. Harten, 'High resolution schemes for hyperbolic conservation laws', *J. Comput. Phys.*, **49**, 357 (1983).
3. P. L. Roe, 'Approximate Riemann solvers, parameter vectors, and difference schemes', *J. Comput. Phys.*, **43**, 357 (1981).
4. P. L. Roe and J. Pike, 'Efficient construction and utilisation of approximate Riemann solutions', *Computing Methods in Applied Science and Engineering VI*, p. 499 1984.
5. P. K. Sweby, 'High resolution schemes using flux limiters for hyperbolic conservation laws', *SIAM J. Numer. Anal.*, **21**, 995 (1984).
6. P. Glaister, 'Flux difference splitting for the Euler equations in non-Cartesian geometry', *Numerical Analysis Report 8-85*, University of Reading, 1985.
7. P. Glaister, 'An approximate linearised Riemann solver for the Euler equations in one dimension with a general equation of state', *Numerical Analysis Report 7-86*, University of Reading, 1986.
8. P. L. Roe, 'Upwind differencing schemes, hyperbolic conservation laws with source terms', in C. Carassa and D. Serre (eds), *Proc. 1st Int. Congr. on Hyperbolic Problems*, St. Etienne, 1986.
9. P. K. Sweby, 'A modification of Roe's scheme for entropy satisfying solutions of scalar non-linear conservation laws', *Numerical Analysis Report 6-82*, University of Reading, 1982.
10. W. F. Noh, 'Artificial viscosity (Q) and artificial heat flux (H) errors for spherically divergent shocks', *UCRL Preprint 89623*, 1983.
11. M. Ben-Artzi and J. Falcovitz, 'An upwind second-order scheme for compressible duct flows', *SIAM J. Sci. Stat. Comput.*, (to appear), 1983.